Mapping of Mechanical Strains and Stresses around Quiescent Engineered Three-Dimensional Epithelial Tissues

Nikolce Gjorevski[†] and Celeste M. Nelson[†‡]

[†]Department of Chemical and Biological Engineering, and [‡]Department of Molecular Biology, Princeton University, Princeton, New Jersey

SUPPORTING MATERIALS AND METHODS

Scanning electron microscopy (SEM)

The internal structure of the collagen gels (formed as described above) was visualized using SEM. The gels were prepared for SEM by fixation, followed by serial dehydration. Specifically, the samples were fixed in 4% paraformaldehyde for 1 h at room temperature, and then washed with ddH_2O twice for 10 min. The samples were then subjected to serial dehydration using an ethanol/ddH_2O series: 30%, 50%, 70%, 90% and two 100% ethanol washes for 10 min each. The samples were subsequently washed using a graded ethanol/HMDS series: 33%, 50%, 66% and 100% HMDS washes for 15 min each. Finally, the gels were cut and dried overnight with their cross-section facing up. The dried samples were mounted on SEM sample stubs using carbon tape and coated with Pd/Au to a thickness of 6 nm using a Denton Vacuum Desk II sputter coater (Denton Vacuum). The samples were imaged at 5,000× and 10,000× magnification using a JEOL 840 SEM (JEOL Ltd.) The average pore size within three separate 5 μm × 5 μm regions of the three different gels was measured manually in ImageJ (NIH) (**Fig. S4**). Keeping in mind that the average pore size of the gel (~100 nm) was significantly smaller than both the beads (1 μm), the average distance between the beads (17±4 μm), and the smallest dimension of the force-applying epithelial tissues (50 μm), we modeled the collagen gel as a continuous medium (1).

Measurement of Darcy permeability and estimation of pore size

To verify the accuracy of the pore size of the collagen gels as measured by SEM, we calculated the pore size analytically. The permeability of the collagen gel was measured by monitoring the flow rate of water through microfabricated channels of collagen under a known hydrostatic pressure. Channels within PDMS chambers (cross-sectional area of 1 mm^2 and length of 1 cm) were formed using standard lithographic techniques and filled with collagen. Flow rates induced by a hydrostatic pressure of 1 cm H_20 were measured. The Darcy permeability (K) of the sample was determined from the flow rates and the geometric features of the apparatus, using Darcy's law:

$$Q = K\frac{A}{L}\frac{\Delta P}{\mu} \tag{1}$$

where Q is the flow rate, A is the cross-sectional area of the channel, L is the length of the channel, ΔP is the pressure drop and μ is the viscosity of water. Our measurements yield a permeability constant of 0.070±0.016 μm^2 for the collagen gels used in this study.

We estimated the fiber diameter of the gels by using the empirical form of the Spielman-Goren fiber matrix model, which describes the transport properties of a random fibrous network (2):

$$K = 0.31a^2\phi^{-1.17} \tag{2}$$

where a is the fiber radius and ϕ is the solid fraction of the gel, obtained by multiplying the collagen concentration with the effective specific volume of collagen, reported previously as 1.89 ml/g (3). We estimated a fiber diameter of 54±6 nm, which is in reasonable agreement with the fiber sizes measured from the SEM images.

Finally, we used the Carman-Kozeny model (4, 5) to estimate the pore size of the collagen gel:

$$K = \frac{\varepsilon m^2}{4k} \tag{3}$$

Here, $m = (b^2 - a^2)/2a$, where b is the pore size. This model treats the gels as a mesh of cylinders, randomly oriented in three dimensions and described by a geometric factor k:

$$k = (2k_{+} + k_{\parallel}) \tag{4}$$

where:

$$k_{\parallel} = \frac{2\varepsilon^3}{(1-\varepsilon)\left[2\ln\left(\frac{1}{1-\varepsilon}\right) - 3 + 4(1-\varepsilon) - (1-\varepsilon)^2\right]} \tag{5}$$

$$k_{+} = \frac{2\varepsilon^3}{(1-\varepsilon)\left[\ln\left(\frac{1}{1-\varepsilon}\right) - \frac{1-(1-\varepsilon)^2}{1+(1-\varepsilon)^2}\right]} \tag{6}$$

The porosity of the gel ε is related to the solid fraction by the equation ε=1-ϕ. Using Eqs. 3-6, we estimated a pore size of 435±26 nm. This calculated pore size is of the same order of magnitude as that obtained through analysis of the SEM images.

Characterization of collagen layer adhesion

The 3D collagen gel surrounding the tissue was prepared in a layer-by-layer fashion, as described in the main text. To confirm that the two collagen layers were integrated mechanically, we embedded beads of different colors into each layer before microfabrication, which allowed us to distinguish between displacements induced by the tissue in each domain separately (**Fig. S1**). By visual inspection, the displacement field propagated smoothly and continuously across the boundary from the bottom to the top layer. Consistently, the x-, y- and z-displacements were a continuous function of depth, with no discontinuities or jumps apparent at the boundary between the layers (**Fig. S1 *A***). Moreover, the displacement profiles were symmetric about the midsection of the tissue in the z-direction, i.e. displacements around the interface between the two layers were similar to those at the same depth below the tissue, where the gel is truly continuous. In a small fraction (<5%) of all microfabrication experiments, the gels failed to bind fully, owing to a film of liquid trapped between the two layers. Such cases were readily identifiable, as the cells failed to form a quiescent epithelial tubule and instead migrated as monolayers between the two gels (**Fig. S1 *B***). An asymmetric displacement profile was recorded within gels in which the top and bottom layers were detached. The bottom layer was displaced dramatically, whereas negligible displacements were observed in the top layer. (**Fig. S1 *C***).

Confocal reflection microscopy

The structure of the collagen around the tissues was visualized using a Leica SP5 laser-scanning confocal microscope. Collagen matrices were illuminated with an Argon laser (488 nm) and imaged in reflection mode using a 20× oil-immersion objective. Images of the collagen surrounding 20 tissues or cell-free collagen cavities were taken at a z-position corresponding to the middle of the tissue or well. The raw intensities of the 20 images were averaged using ImageJ and color-coded using Adobe Photoshop to generate color maps of reflection signal intensity.

Atomic force microscopy (AFM)
AFM analyses to probe the local elasticity of collagen gels were performed on an MFP 3D system (Asylum Research) in a liquid environment to prevent drying of the gel. Force measurements were conducted using cantilevers with low spring constants (k=0.05 N/m; MikroMasch). After initial contact with the surface of the collagen gel, force vs piezo displacement (F-z) data were collected at a speed of 1 Hz for a total z-distance of 4 μm. Since the tissues have two axes of symmetry, only the upper left quadrant was scanned with a resolution of ~10 μm. Three F-z curves were recorded at each location probed. Young's moduli were computed using the Elastic algorithm for a pyramidal tip (Igor Pro; Wavemetrics). Indentation measurements to compare the elasticity of the gel near the side and the end of the tissue were performed on five separate samples, and full elasticity maps were generated for three separate samples. Magnitudes and distribution of elasticity were highly reproducible between samples.

Immunofluorescence analysis
Detection of E-cadherin, F-actin, and EdU incorporation was performed as described (6). In brief, for immunofluorescence analysis of E-cadherin and F-actin, samples were washed in PBS, fixed in 4% paraformaldehyde, permeabilized with 0.1% Triton-X-100 in PBS, and blocked in 10% goat serum in PBS. Samples were incubated overnight in primary antibody against E-cadherin (Cell Signaling), washed extensively, and then visualized using a secondary antibody or fluorescently-conjugated phalloidin (Invitrogen).

Proliferating cells were detected using the Click-iT EdU Imaging Kit (Invitrogen) per manufacturer's instructions. Frequency maps of proliferating cells were constructed by stacking fluorescence images in registration as described previously (6).

SUPPORTING REFERENCES

1. Koch, T. M., S. Munster, N. Bonakdar, J. P. Butler, and B. Fabry. 2012. 3D Traction Forces in Cancer Cell Invasion. PloS one 7:e33476.
2. Ethier, C. R. 1986. The Hydrodynamic Resistance of Hyaluronic-Acid - Estimates from Sedimentation Studies. Biorheology 23:99-113.
3. Levick, J. R., and L. H. Smaje. 1987. An analysis of the permeability of a fenestra. Microvasc Res 33:233-256.
4. Happel, J. 1959. Viscous Flow Relative to Arrays of Cylinders. Aiche J 5:174-177.
5. Ramanujan, S., A. Pluen, T. D. McKee, E. B. Brown, Y. Boucher, and R. K. Jain. 2002. Diffusion and convection in collagen gels: Implications for transport in the tumor interstitium. Biophys J 83:1650-1660.
6. Gjorevski, N., and C. M. Nelson. 2010. Endogenous patterns of mechanical stress are required for branching morphogenesis. Integr Biol (Camb) 2:424-434.

Figure S1

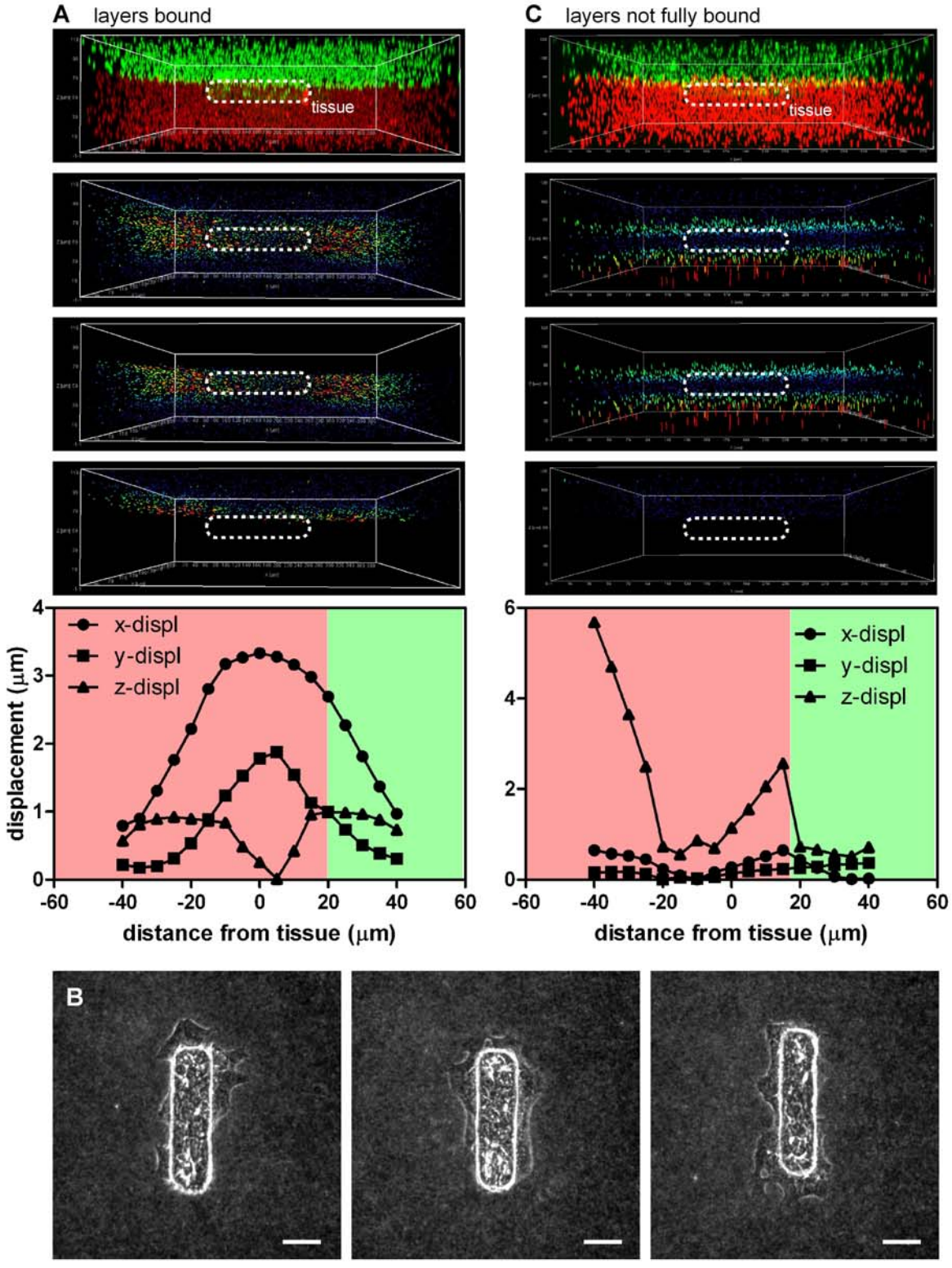
A layers bound
tissue
C layers not fully bound
tissue
x-displ
y-displ
z-displ
displacement (μm)
distance from tissue (μm)
x-displ
y-displ
z-displ
distance from tissue (μm)
B

Fig. S1. The physical integrity of the collagen matrix was validated by loading the two layers with beads of different colors, and tracking the tissue-induced displacements of the layers separately. (*A*) In fully bound collagen gels, tissue-induced displacements propagated smoothly, with no apparent jumps or discontinuities at the boundary between the top and bottom layers. (*B*) Physical detachment of the top and bottom layers, which occurs but rarely (<5% of samples), is accompanied by a distinct cellular phenotype: cells fail to reorganize into quiescent epithelial tubules, and migrate as monolayers out of the wells, between the two collagen layers. (*C*) An asymmetric displacement profile was recorded within gels in which the top and bottom layers were detached. The bottom layer was displaced dramatically, whereas negligible displacements were observed in the top layer. Scale bars, 50 μm.

Figure S2

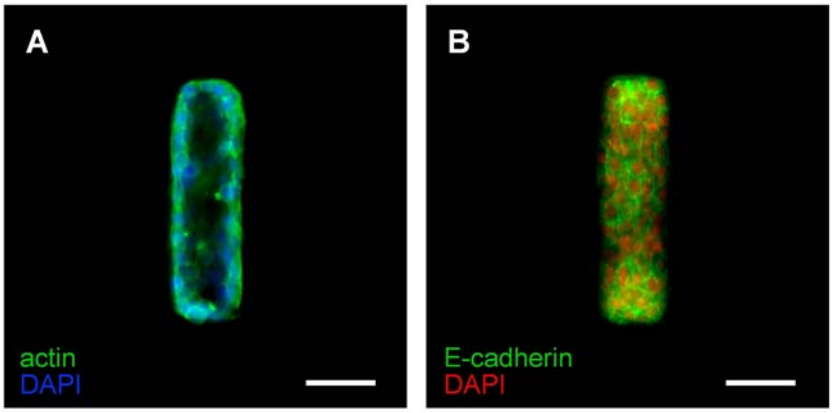

Fig. S2. Internal and surface structure of engineered mammary epithelial tissues. (*A*) Confocal section of a representative mammary epithelial tissue stained for actin (green) and DNA (blue). (*B*) Surface of a representative tissue stained for E-cadherin (green) and DNA (red). Scale bars, 50 μm.

Figure S3

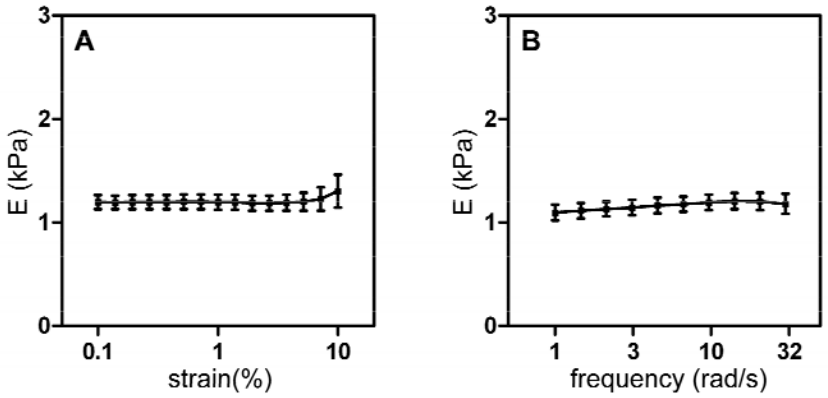

Fig. S3. Mechanical characterization of collagen gels. (*A*) Plot of the Young's modulus, calculated from the shear modulus *G'* with a Poisson ratio of 0.2, as a function of applied strain. The tissue-induced strain values at most locations throughout the gel fell below 5%, and a maximum strain of 7% was recorded. (*B*) Plot of the Young's modulus as a function of frequency. Measurements were conducted at applied strain of 1%. The Young's modulus of the collagen gels is not influenced significantly by applied strain magnitude or frequency. Plots show average ± SEM.

Figure S4

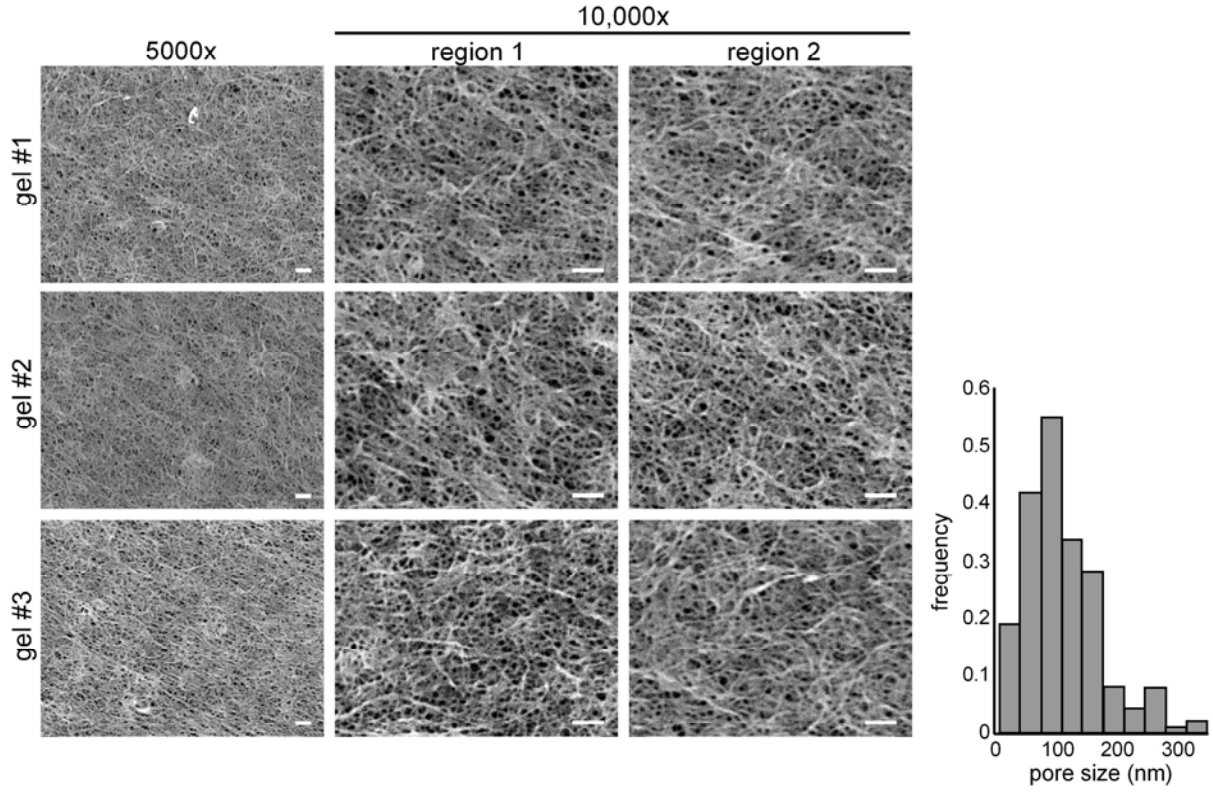

Fig. S4. Scanning electron micrographs depicting the internal structure of the collagen gels. The average pore size within three separate regions (5 μm × 5 μm) of the three different gels was measured manually in ImageJ, and the resulting distribution was represented as a histogram. Scale bars, 1 μm.

Figure S5

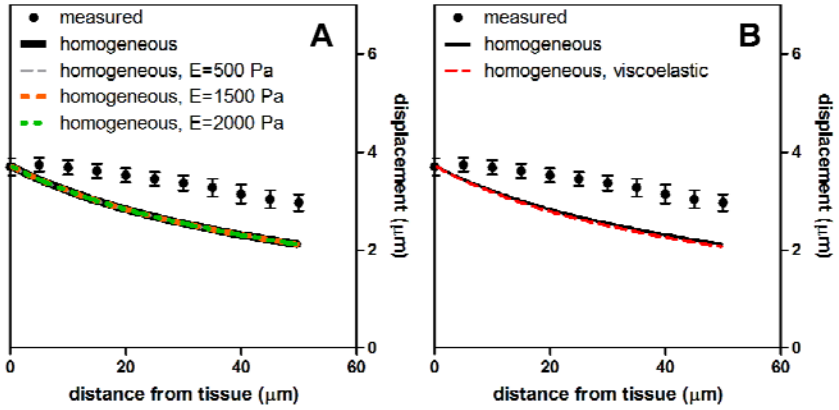

Fig. S5. Effect of error in material properties and choice of constitutive model for collagen on calculation of stress. (*A*) Comparison of matrix deformation measured experimentally and deformation simulated in homogeneous, elastic material of varying material properties. (*B*) Comparison of matrix deformation measured experimentally and deformation simulated in homogeneous, viscoelastic material. Viscoelastic parameters were determined by fitting the two-mode Maxwell mode to the experimental *G'* vs frequency data obtained by bulk rheometry.

Figure S6

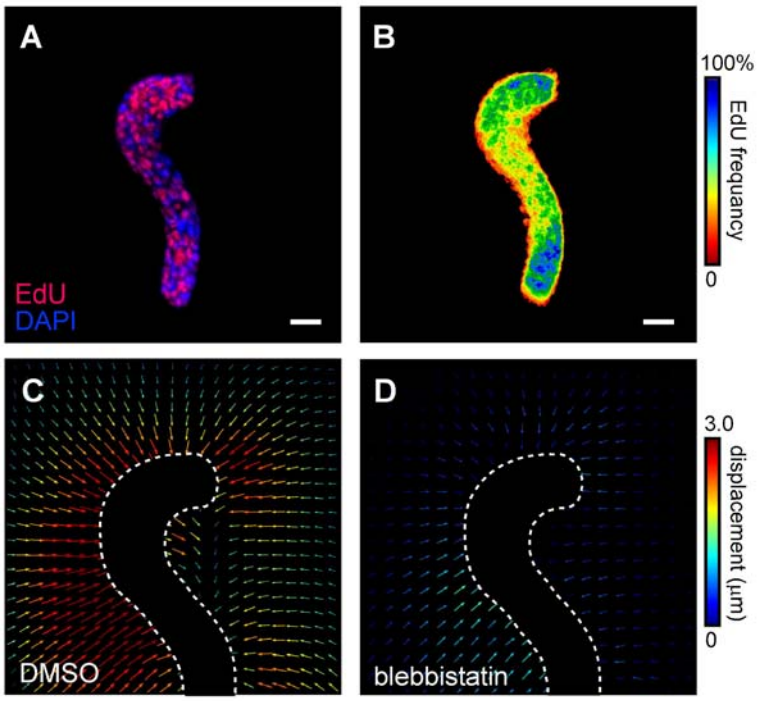

Fig. S6. Emergent compression in epithelial tissues is driven by actomyosin-mediated contractility and not localized proliferation. (*A*) Immunofluorescence image and (*B*) frequency map showing the spatial distribution of EdU incorporation within engineered tissue containing regions of convex and concave curvature. (*C*) A map of average matrix displacements around multiple (n=17) control tissues treated with DMSO. (*D*) A map of average matrix displacements around multiple (n=17) tissues treated with blebbistatin (25 μM). Scale bars, 50 μm.